Critical Trapping Numbers and Capillary Desaturation in Mixed-to-Oil-Wet Carbonates under High-Temperature, High-Salinity Surfactant Flooding

Imad A. Adel[a], Alvaro Hernandez Moralez[a], Mohamed Efara[a], Emad W. Al-Shalabi[a,b], Ali AlSumaiti[c], Shehadeh Masalmeh[c]

[a] *Chemical and Petroleum Engineering Department, Khalifa University of Science and Technology, Abu Dhabi, United Arab Emirates*

[b] *Research and Innovation Center on CO_2 and Hydrogen (RICH), Khalifa University of Science and Technology, Abu Dhabi, United Arab Emirates*

[c] *Abu Dhabi National Oil Company (ADNOC), Abu Dhabi, United Arab Emirates*

** Manuscript under review at **Geoenergy Science and Engineering** (Elsevier).*

Abstract

This study reports capillary desaturation curves (CDCs) for two crude-oil-aged carbonate systems with expected mixed-to-oil-wet behavior—a Middle East reservoir core plug and an Indiana Limestone outcrop analogue—at 100 °C and 243,028 ppm TDS connate-water salinity. Prior to tertiary injection, each core was centrifuge-conditioned to establish a less end-effect-biased residual-oil baseline (S_{orw}) for CDC construction. We quantify the critical trapping number ($N_{t,crit}$) and the desaturation response using a multi-rate flooding protocol. Each experiment comprised a synthetic seawater pre-flush (43,373 ppm TDS), followed by a near-optimal surfactant flood formulated in seawater. The surfactant blend (Guerbet alkoxy carboxylate (GAC) and internal olefin sulfonate (IOS)) yields an ultra-low interfacial tension σ_{os}(100 °C) = 3.07 × 10^{-3} mN/m. In the reservoir core plug ($k_{w,Sorw}$ = 2.24 mD), surfactant flooding reduced oil saturation from S_{orw} = 40% to S_{orc} = 7.2%, yielding $N_{t,crit}$ = 2.23 × 10^{-3}. In the Indiana Limestone outcrop ($k_{w,Sorw}$ = 74.93 mD), oil saturation decreased from S_{orw} = 16.5% to S_{orc} = 9.5%, yielding $N_{t,crit}$ = 8.47 × 10^{-4}. These measured mobilization thresholds are substantially higher than a classical water-wet sandstone baseline (~10^{-5}), indicating that direct transfer of water-wet CDC criteria can underrepresent the mobilizing force required for the tested aged carbonates. Under the adopted field-rate scaling, ultra-low IFT at u = 1 ft/day gives $N_t \approx 2.09 \times 10^{-3}$ for the reservoir carbonate, which is slightly below the measured RC onset and provides limited margin for deeper desaturation. For the tested low-permeability reservoir carbonate, viscosity enhancement remains a screening variable for higher trapping-number targets, subject to injectivity, polymer propagation, retention, and fracture-pressure constraints. These results provide carbonate-specific CDC and $N_{t,crit}$ benchmarks for screening surfactant flooding in mature HTHS carbonate reservoirs, where direct transfer of water-wet correlations may underrepresent the mobilizing force required.

Keywords

Surfactant flooding; Capillary desaturation curve; Trapping number; Mixed-wet carbonate; HTHS chemical EOR; Centrifuge conditioning; Mature carbonate reservoirs

1. Introduction

Trapped oil mobilization in carbonates is governed by capillary forces, which retain oil in pores, and viscous and gravitational forces. The capillary number N_c quantifies the dimensionless ratio of viscous to capillary forces [1,2]. In surfactant enhanced oil recovery (EOR), residual-oil mobilization is commonly evaluated from capillary desaturation behavior, in which IFT reduction increases the applied mobilizing force when the desaturation threshold is exceeded [3,4]. To account for gravitational contributions, the Bond number N_b defines the ratio of buoyancy to capillary forces. Following Pope et al. [12] (originally developed for gas-condensate systems but applicable to oil-water displacement under the same dimensionless-number framework), the total trapping number N_t vectorially combines N_c and N_b to represent the total mobilizing force. Reliable carbonate-specific mobilization thresholds are therefore relevant to mature-reservoir recovery efficiency and sustainable hydrocarbon production.

Capillary trapping and desaturation depend strongly on wetting state and pore architecture. In classical, strongly water-wet systems, residual oil is predominantly trapped as discontinuous ganglia within larger pore bodies via snap-off and bypassing mechanisms at pore constrictions [18,20]. Mobilization of these isolated ganglia typically begins over a narrow threshold near $N_{t,crit}$ = 1 × 10^{-5}–2 × 10^{-5} [2]. This water-wet paradigm does not transfer directly to non-water-wet carbonates. Mixed-to-oil-wet carbonate surfaces can retain oil in smaller pores, micro-porosity, and continuous wetting films on the rock matrix [5]. Displacement therefore requires overcoming higher capillary resistance associated with film drainage [6].

As wettability departs from strongly water-wet conditions, the capillary desaturation curve (CDC) can shift to higher mobilizing forces. Masalmeh [5] and Humphry et al. [6] showed that mobilization thresholds in non-water-wet rocks can increase by orders of magnitude, placing $N_{t,crit}$ within the 10^{-4} to 10^{-2} range depending on rock type, wettability, and experimental protocol. At standard reservoir Darcy

velocities (e.g., u = 1 ft/day), generating these mobilizing forces through viscous pressure gradients alone may be operationally constrained. Direct transfer of water-wet sandstone CDC correlations to mixed-wet carbonate systems can, therefore, underrepresent the mobilizing force required for tertiary recovery.

Critical gaps remain in published N_t-based desaturation scaling. First, executing the extended multi-rate protocols required to establish CDCs under severe HTHS conditions is experimentally challenging due to surfactant degradation, divalent-ion precipitation, and phase-behavior instability over the extended laboratory timeframes required to reach steady-state [7,8].

Second, historical CDC datasets frequently define S_{orw} using waterflood endpoints obtained at low laboratory pressure gradients. As demonstrated by Masalmeh [5], low-rate waterfloods in mixed-to-oil-wet rocks can terminate at an apparent remaining oil saturation rather than a lower residual-oil baseline. This apparent saturation may be inflated by capillary end effects at the outlet boundary and by very low oil relative permeability (k_{ro}) near residual conditions. If this remaining saturation is used as the CDC baseline, the resulting critical trapping number may be biased downward and chemical-EOR screening forecasts may become optimistic. High-speed centrifuge conditioning provides a mechanical route to reduce this boundary artifact by imposing a more controlled outflow condition [9]; it was therefore used here to condition the plugs to the reference S_{orw} before tertiary injection.

Third, rigorously conditioned CDC datasets for aged or mixed-wet rocks under HTHS conditions remain limited compared with classical strongly water-wet sandstone datasets and recent carbonate surfactant-EOR studies have continued to emphasize permeability dependence, wettability alteration, adsorption, and recovery response rather than directly measured trapping-number thresholds [24–26]. Consequently, reservoir models and chemical-EOR screening workflows may default to published water-wet desaturation correlations (e.g., [2]) when evaluating mobilization in carbonates. This transfer is not generally conservative for mixed-wet systems because the mobilization threshold depends on wettability, pore architecture, residual-oil baseline definition, and the velocity convention used in the dimensionless number.

To address these gaps, this study reports centrifuge-conditioned CDCs and $N_{t,crit}$ values for a low-permeability reservoir carbonate (RC) and a higher-permeability Indiana Limestone outcrop analogue (IL) at 100 °C. We used a Guerbet alkoxy carboxylate (GAC) and internal olefin sulfonate (IOS) blend (SF1) with $\sigma_{os}(100\ °C) = 3.07 \times 10^{-3}$ mN/m, extrapolated from spinning-drop measurements up to 90 °C. Each plug was centrifuge-conditioned to establish the reference S_{orw} prior to chemical injection, and a stepwise, multi-rate flooding protocol was then applied at ultra-low IFT. The objective is to isolate the N_t-controlled desaturation response from macroscopic end-effect bias and to evaluate how the measured thresholds affect surfactant-EOR screening at field-representative Darcy velocities.

2. Methodology

2.1. Materials.

Aqueous Phase Composition. We synthesized aqueous phases by dissolving analytical-grade salts—sodium chloride (NaCl), calcium chloride dihydrate ($CaCl_2 \cdot 2H_2O$), magnesium chloride hexahydrate ($MgCl_2 \cdot 6H_2O$), sodium sulfate (Na_2SO_4), and sodium bicarbonate ($NaHCO_3$)—into deionized water (resistivity ≥ 18.2 MΩ·cm). We used two brine compositions:

- Seawater (SW): The injection base fluid and solvent for the surfactant slug. Total Dissolved Solids (TDS) was fixed at 43,373 ppm, replicating the field injection source.
- Formation Water (FW): Synthesized with 243,028 ppm TDS and high divalent ion content to simulate connate water saturation.

The ionic compositions and physical properties of both brines are summarized in Table 1. These formulations were used throughout the coreflood program.

Table 1. Properties and Ionic Composition of Synthetic Formation Water (FW) and Injection Seawater (SW)

Ion	FW	SW
Na^+	66,130	13,662
Ca^{2+}	23,246	539
Mg^{2+}	2,674	1,583
K^+	—	498
Cl^-	150,675	27,092
SO_4^{2-}	230	0
HCO_3^-	—	0
Br^-	—	0
I^-	—	0
TDS (ppm)	243,028	43,373

Property	FW	SW
Total dissolved solids (ppm)	243,028	43,373
Hardness (ppm as $CaCO_3$)	26,520	2,122
Viscosity (cP)	1.57	1.02
Density (g/cm^3)	1.17	1.04

Note: Density and viscosity values are reported at ambient conditions (25 °C, 1 atm).

Reservoir Crude Oil. We used stock-tank crude oil from the target Middle Eastern carbonate reservoir. The crude underwent a conditioning protocol: mechanical centrifugation to remove basic sediments and water, filtration through a 0.5-micron inline filter to eliminate suspended asphaltene aggregates, and vacuum-degassing. Rheological characterization established a dead oil viscosity of 1.25 cP at 100 °C.

Surfactant Formulation. We used Formulation SF1 to maintain aqueous compatibility and interfacial activity under the HTHS conditions evaluated here. The primary surfactant was a sodium Guerbet alkoxy carboxylate (C24–35PO–30EO–COONa) at 0.5 wt% active matter basis. Internal olefin sulfonates (IOS 15–18 and IOS 20–24 sodium salt) were used as co-surfactants to broaden the Winsor Type III microemulsion window [10]. An ethoxylated phenol co-solvent (0.5 wt% active basis) was included to reduce interfacial rigidity, suppress macroemulsions, and accelerate equilibration kinetics [11]. All reported concentrations are normalized to active matter content.

Porous Media Characterization. We selected two carbonate plugs spanning a wide permeability range to compare CDC response under identical chemistry and temperature. The cores were used as contrasting end-members for this screening study: a low-permeability reservoir sample (~2 mD effective water permeability at S_{orw}) and a higher-permeability Indiana Limestone outcrop analogue (~75 mD effective water permeability at S_{orw}).

- Reservoir Carbonate (RC): A reservoir carbonate core plug from a low-permeability interval ($k_{w,Sorw}$ = 2.24 mD, ϕ = 0.22)
- Outcrop Carbonate (IL): A moderate-to-high-permeability Indiana Limestone outcrop ($k_{w,Sorw}$ = 74.93 mD, ϕ = 0.18)

Prior to dynamic testing, the plugs underwent petrophysical preparation. The samples were trimmed, cleaned to remove residual fluids, and oven-dried to establish baseline porosity. Following vacuum saturation with formation water (FW), the absolute brine permeability, k_b, was measured. Primary drainage was then conducted using the filtered reservoir crude oil to establish the initial water saturation S_{wi}. To promote a representative aged carbonate wetting state, the plugs were submerged in crude oil within pressurized aging cells and thermally aged at 100 °C for three weeks. The wetting state was inferred from the aging protocol and displacement-response interpretation, not independently quantified by Amott, USBM, or contact-angle measurements. Core dimensions and petrophysical properties are listed in Table 2.

Table 2. Core Dimensions and Petrophysical Properties

Core ID	Length (cm)	Diameter (cm)	PV (cm^3)	k_b (mD)	$k_{w,Sorw}$ (mD)	ϕ (frac.)	S_{wi} (frac.)	S_{orw} (frac.)
RC	5.13	3.75	12.11	10.07	2.24	0.22	0.23	0.40
IL	4.99	3.80	9.58	97.58	74.93	0.18	0.31	0.165

2.2. Experimental Procedures. Dynamic displacement experiments used a HPHT coreflood system, a confining pressure of 1200 psi and back pressure of 200 psi, temperature control at 100 °C, differential pressure monitoring, and back-pressure regulation.

2.3. Residual Oil Conditioning and Centrifuge Data Interpretation.

To establish a residual-oil baseline less affected by capillary end effects, each plug was conditioned using a multispeed centrifuge prior to the tertiary sequence [5]. At each rotational speed, fluid production was monitored until an equilibrium plateau was reached. The S_{orw} values reported prior to chemical injection are therefore treated as centrifuge-conditioned reference baselines for CDC construction, not as universal residual saturations independent of protocol and rock type.

Dynamic Desaturation via Stepwise Coreflooding and Trapping Number Formulation. Following centrifuge conditioning to the reference S_{orw}, we used a dynamic coreflooding protocol to evaluate desaturation under controlled increases in mobilizing force. We quantify the total mobilizing force using the trapping number (N_t), which vectorially combines the capillary number (N_c) and Bond number (N_b) [12]. In this study, u denotes Darcy (superficial) velocity and $v = u/\phi$ denotes interstitial velocity. The viscous component is evaluated on an interstitial-velocity basis, so that $N_c = v\mu/\sigma = u\mu/(\phi\sigma)$. This convention is used consistently for the laboratory and field-rate scaling calculations; benchmark comparisons are converted to the same basis before interpretation.

$$N_c = \frac{v \cdot \mu}{\sigma} = \frac{u \cdot \mu}{\phi \cdot \sigma} \tag{1}$$

where v is the interstitial velocity, u is the Darcy (superficial) velocity, μ is the viscosity of the displacing aqueous phase, σ is the interfacial tension, and ϕ is the porosity. At 100 °C, μ is 0.40 cP for both seawater and the SF1-in-seawater solution; the surfactant formulation did not measurably change the aqueous baseline viscosity. By defining μ as the aqueous displacing-phase viscosity, the applied viscous force is referenced to a defined fluid property rather than to the complex, shear-dependent microemulsion viscosities that may form in situ.

$$v = \frac{u}{\phi} \tag{2}$$

The Bond number N_b defines the ratio of buoyancy to capillary forces and is calculated using Eq. (3):

$$N_b = \frac{\Delta\rho \cdot g \cdot k_{w,Sorw}}{\phi \cdot \sigma} \tag{3}$$

where $\Delta\rho$ is the density difference between the aqueous and oleic phases (200 kg/m^3), g is gravitational acceleration (9.81 m/s^2), $k_{w,Sorw}$ is the effective permeability to water at residual oil saturation, and ϕ is the porosity.

For the baseline N_c and N_b calculations, the wettability term ($\cos\theta$) is omitted (effectively set to unity) to isolate the applied mechanical viscous and buoyancy forces from rock-fluid interaction terms. The N_b formulation (Eq. (3)) follows the Masalmeh [5] definition ($N_b = k_{w,Sorw}\Delta\rho g / \phi\sigma \cos\theta$), which places the buoyancy term on the same interstitial basis as the viscous term in Eq. (1), so that the two combine consistently in Eq. (5). It differs by a factor of $1/\phi$ from the Pope et al. [12] convention, which omits porosity from the denominator. Incorporating in situ contact angle can be necessary when the objective is to represent the apparent capillary resistance of mixed-to-oil-wet systems. The simplified formulation adopted here should therefore be interpreted as a defined mechanical baseline rather than a complete wettability-dependent trapping criterion. The trapping number N_t vectorially combines these forces using Eq. (4):

$$N_t = \sqrt{{N_c}^2 + 2\,N_c\,N_b\,\sin\alpha + {N_b}^2} \tag{4}$$

For the horizontal displacement configuration used in this study ($\alpha = 0°$), N_t reduces to Eq. (5):

$$N_t = \sqrt{{N_c}^2 + {N_b}^2} \tag{5}$$

To map the capillary desaturation curve, we applied a stepwise injection protocol that incrementally escalated the applied N_t on a single sample. Each rate step was maintained for at least 1.5 pore volumes and continued until both differential pressure and effluent fractional flow approached stable values. Because the onset criterion depends on measurable oil production, $N_{t,crit}$ is reported operationally as the highest tested trapping number before measurable desaturation.

The protocol advanced through the following defined stages:

- Baseline Conditioning: Prior to surfactant injection, each core was flooded with seawater to establish the injection salinity and confirm a stable reference residual-oil baseline. Seawater was injected over a sequence of flow rates, after which the rate was returned to 0.25 cm^3/min before surfactant injection. No incremental oil was produced at this reference rate, supporting use of the centrifuge-conditioned baseline for the tertiary desaturation sequence.
- Surfactant Injection: The IFT of formulation SF1 is $\sigma_{os} \approx 3.07 \times 10^{-3}$ mN/m. Once the oil cut ceased at the lowest reference rate, the injection flow rate was increased to Q = 0.075, 0.25, 0.5, 1, 2, 6, 8, and 12 cm^3/min. Each rate plateau was maintained

for a minimum of 1.5 pore volumes, and the rate was increased only after the differential pressure (ΔP) and effluent fractional flow approached stable values.

- Salinity-Gradient Post-Flush: Following the maximum applied viscous pressure-gradient step, a seawater chase and a subsequent 50% diluted-salinity brine (Q = 0.25 cm^3/min) were injected. Because this step was executed at low flow rate, it was used to probe whether phase-behavior changes could mobilize additional oil without increasing mechanical forcing. The interpretation is therefore limited to a phase-behavior-related response consistent with a shift from near-optimum Winsor Type III conditions toward under-optimum Winsor Type I conditions [13,14].

Uncertainty in the trapping-number estimates is dominated by the adopted oil–surfactant IFT. The oil–surfactant IFT, σ_{os}, was measured by spinning-drop tensiometry up to 90 °C and extrapolated to 100 °C using a power-law regression (R^2 = 0.994); the independent Huh-derived estimate, σ_{Huh} = 3.32 × 10^{-3} mN/m, differs by ~8% from the extrapolated σ_{os}(100 °C) = 3.07 × 10^{-3} mN/m. Because N_t is inversely proportional to σ, a ±20% uncertainty in σ propagates to a ±20% uncertainty in $N_{t,crit}$; for Core RC this gives a propagated range of approximately (1.78–2.68) × 10^{-3}, and for Core IL approximately (6.78 × 10^{-4} – 1.02 × 10^{-3}). Separately, the operational definition of $N_{t,crit}$ places an empirical bracket between the highest tested trapping number before measurable desaturation and the next rate step at which oil was produced; this empirical bracket spans 2.23 × 10^{-3} to 4.47 × 10^{-3} for Core RC and 8.47 × 10^{-4} to 2.69 × 10^{-3} for Core IL.

3. Results and Discussion

3.1. Phase Behavior and Interfacial Tension Validation. Formulation SF1 was characterized under HTHS conditions to confirm aqueous stability and Winsor Type III microemulsion formation near the injection salinity (43,373 ppm TDS). Salinity scans at 100 °C demonstrated a Type I to Type III to Type II phase transition. The aqueous stability limit extended to 70,000 ppm, establishing a margin above the injection salinity. At the optimal salinity (S^* = 45,000 ppm), the formulation exhibited an optimal solubilization ratio (R^*) of 9.5 cm^3/cm^3. A summary of SF1 fluid properties and phase behavior at 100 °C is listed in Table 3.

Table 3. Summary of SF1 Fluid Properties and Phase Behavior at 100 °C

Parameter	Value	Unit
Optimal salinity (S^*)	45,000	ppm TDS
Solubilization ratio (R^*)	9.5	cm^3/cm^3
Calculated IFT, Chun–Huh (σ_{Huh})	3.32 × 10^{-3}	mN/m
Spinning drop IFT (σ_{os})	3.07 × 10^{-3}	mN/m
Baseline, pendant drop (σ_{ow})	24.3	mN/m
Aqueous stability limit	70,000	ppm TDS
Aqueous slug viscosity (μ)	0.40	cP
Microemulsion type	Winsor III	—

Baseline oil–seawater interfacial tension at 100 °C was measured by pendant-drop tensiometry and was 24.3 mN/m. Fig. 1 defines the phase-behavior boundary condition used for SF1. Fig. 1a presents solubilization ratios (V_o/V_s and V_w/V_s) versus salinity, showing a Winsor I to III to II transition. The optimum salinity (S^* = 45,000 ppm) and optimum solubilization ratio (R^* = 9.5 cm^3/cm^3) are close to the injection seawater salinity (43,373 ppm). Fig. 1b shows the interfacial tension (σ_{os}) between the crude oil and the SF1 formulation as a function of temperature, measured by spinning-drop tensiometry.

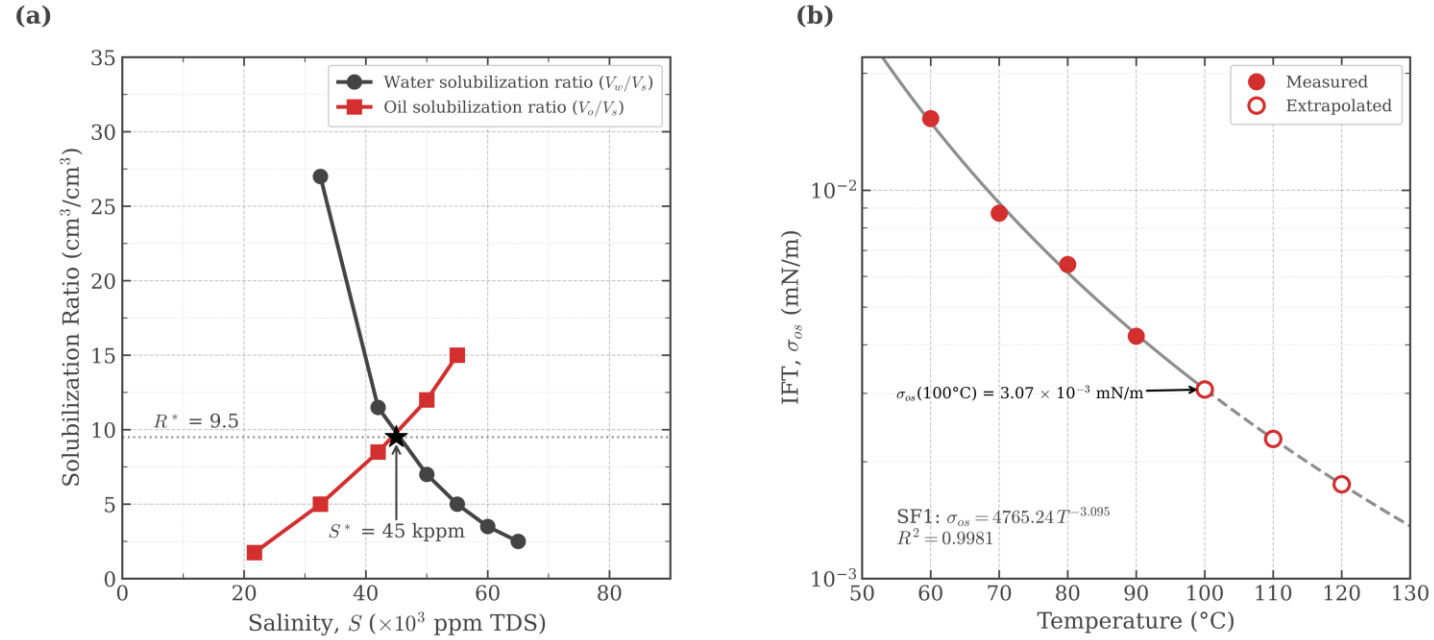

Fig. 1. SF1 phase behavior and oil–surfactant IFT. Panels show (a) solubilization ratios versus salinity and (b) spinning-drop IFT versus temperature.

Measurements were acquired up to 90 °C. The observed temperature trend is consistent with the reported behavior of Guerbet alkoxy carboxylate (GAC) systems, where increasing temperature can shift the formulation toward optimum phase behavior and reduce IFT at fixed salinity and composition [15]. The GAC headgroup is designed for elevated-temperature stability. Therefore, the observed IFT decrease is interpreted as interfacial re-partitioning rather than surfactant loss under the tested conditions. This contrasts with sulfate systems, where hydrolysis can degrade the surfactant and offset IFT reduction [7].

Due to the temperature limit of the available equipment, σ_{os} was extrapolated to 100 °C, 105 °C, and 120 °C using a power-law regression (R^2 = 0.994). This gives σ_{os}(100 °C) = 3.07 × 10^{-3} mN/m for trapping-number calculations. The extrapolation assumes that the same phase environment persists from 90 °C to 100 °C. Surfactant IFT does not necessarily decline monotonically if increasing temperature moves the system across a phase-inversion boundary; such transitions typically yield a V-shaped or U-shaped IFT trajectory rather than a continuous decline [16]. Prior aqueous stability screening showed that the SF1 formulation remained thermally stable and physically homogeneous for at least 21 days at 120 °C. This stability result supports the plausibility of the extrapolated boundary condition, while the uncertainty associated with the above-90 °C extrapolation is treated in Section 2.3. Because N_t is inversely proportional to σ, uncertainty in σ_{os}(100 °C) transfers directly into the calculated trapping numbers.

The Huh equation [17], defined in Eq. (6), provides an independent estimate of interfacial tension from the solubilization ratio at optimum conditions.

$$\sigma = \frac{C}{(R^*)^2} \tag{6}$$

We applied a scaling constant of C = 0.3 mN/m, which is the characteristic value for typical crude oil–surfactant–brine systems [8]. Using C = 0.3 mN/m and R^* = 9.5 cm³/cm³ gives σ_{Huh} = 3.32 × 10^{-3} mN/m. This analytical estimate agrees within 8% of the extrapolated spinning-drop value (σ_{os} = 3.07 × 10^{-3} mN/m at 100 °C). The agreement supports the plausibility of the adopted ultra-low-IFT boundary condition, but it should not be interpreted as independent verification of the temperature extrapolation above the measured range.

3.2. Centrifuge-Conditioned Residual-Oil Baseline. To reduce capillary end-effect bias in the residual-oil baseline, each plug was conditioned using a multispeed centrifuge prior to the tertiary sequence (S_{orw} = 40% for Core RC; 16.5% for Core IL).

3.3. Dynamic Viscous Desaturation Response. Following centrifuge conditioning, the coreflooding experiments progressively increased the trapping number to identify the onset of measurable residual-oil mobilization.

We computed N_t from capillary and buoyancy contributions [12]. For the horizontal configuration (α = 0°), N_t reduces to Eq. (5). We computed N_c using the interstitial-velocity convention defined above ($v = u/\phi$), with μ = 0.40 cP, ϕ = 0.22, and σ_{os}(100 °C) = 3.07 × 10^{-3} mN/m for Core RC. To evaluate mobilization potential under reservoir-rate conditions, the calculation is shown for a standard field Darcy (superficial) velocity of u = 1 ft/day (3.53 × 10^{-6} m/s) for Core RC:

- Darcy velocity (u): 3.53 × 10^{-6} m/s (1 ft/day)

- Interstitial velocity ($v = u/\phi$, Eq. (2)): 1.60×10^{-5} m/s (~4.54 ft/day)
- Viscosity (μ): 0.40 cP (4.0×10^{-4} Pa·s)
- Interfacial tension (σ_{os}): 3.07×10^{-3} mN/m (3.07×10^{-6} N/m)
- $N_c = \frac{v\mu}{\sigma} = \frac{(1.60 \times 10^{-5})(4.0 \times 10^{-4})}{(3.07 \times 10^{-6})} = 2.09 \times 10^{-3}$
- $N_b = 6.42 \times 10^{-6}$
- $N_t = \sqrt{{N_c}^2 + {N_b}^2} = 2.09 \times 10^{-3}$

This calculation shows that at $u = 1$ ft/day, the applied trapping number for Core RC ($N_t \approx 2.09 \times 10^{-3}$) is slightly below the measured onset for this low-permeability reservoir rock ($N_{t,crit} = 2.23 \times 10^{-3}$). Consequently, the multi-rate laboratory protocol increased the injection rate up to 12 cm^3/min ($u = 51.3$ ft/day, $N_t = 1.07 \times 10^{-1}$) to map the complete desaturation trajectory. These elevated N_t steps are laboratory diagnostic endpoints used to define the CDC, not field-gradient targets.

Fig. 2 presents oil saturation as a function of the applied total trapping number. The baseline seawater pre-flush generated no incremental oil, supporting the stability of the centrifuge-conditioned reference S_{orw}.

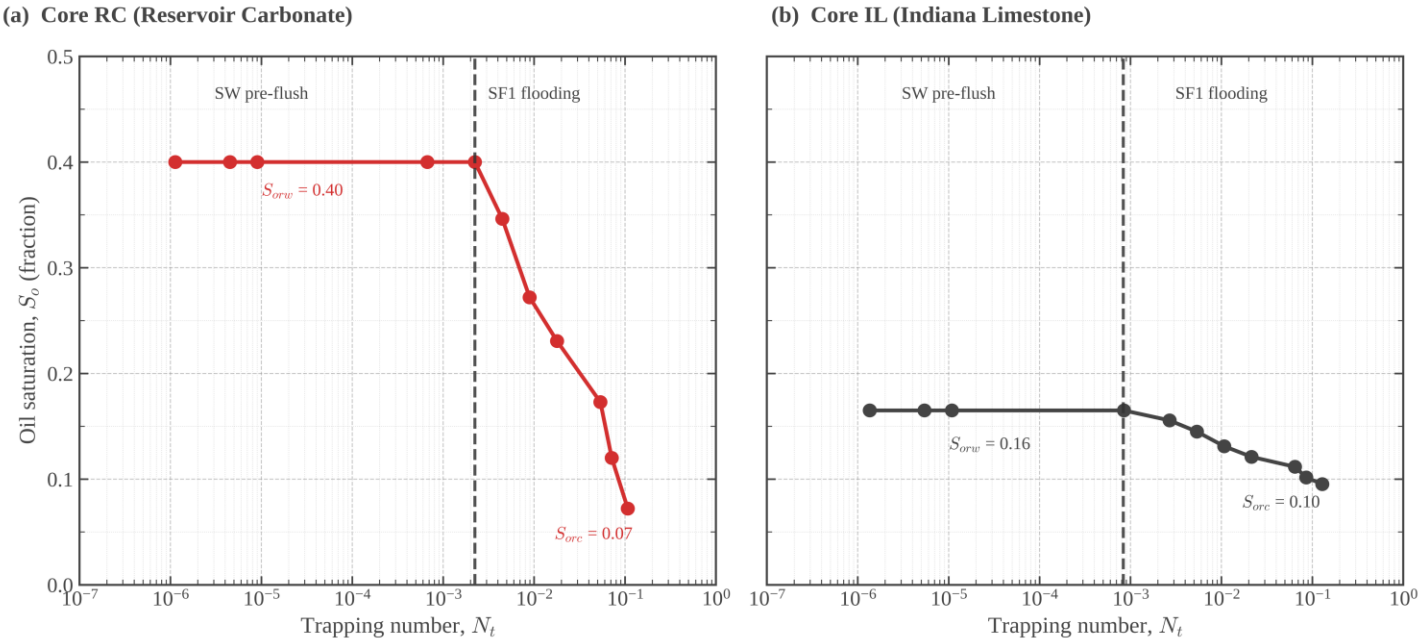

Fig. 2. Oil saturation versus trapping number at 100 °C. Curves show seawater pre-flush endpoints and SF1 rate-escalation desaturation for Cores RC and IL.

During SF1 surfactant injection ($\sigma_{os} = 3.07 \times 10^{-3}$ mN/m), the two lithologies exhibited distinct mobilization thresholds. For the reservoir carbonate (Core RC), the initial ultra-low-IFT injection sequence yielded no measurable desaturation up to $N_t = 2.23 \times 10^{-3}$ ($Q = 0.25$ cm^3/min), and oil was mobilized at $N_t = 4.47 \times 10^{-3}$. The reported critical trapping number is therefore $N_{t,crit} = 2.23 \times 10^{-3}$. Beyond this threshold, desaturation proceeded sharply, reaching $S_{orc} = 7.2\%$ (81.95% of S_{orw} mobilized) at the maximum laboratory viscous limit ($N_t = 1.07 \times 10^{-1}$).

The higher-permeability outcrop analogue (Core IL) exhibited an earlier onset. No measurable desaturation was observed up to $N_t = 8.47 \times 10^{-4}$, defining $N_{t,crit} = 8.47 \times 10^{-4}$. Because Core IL initiated from a much lower S_{orw} of 16.5%, the incremental tertiary recovery was more limited, reaching a terminal S_{orc} of 9.5% (42.22% of S_{orw} mobilized) at the maximum trapping number.

3.4. Water-Wet Sandstone Benchmark as a Screening-Risk Reference. To evaluate the design risk of transferring water-wet CDC criteria to aged carbonate systems, the measured CDCs were benchmarked against a classical water-wet sandstone reference. Fig. 3 presents normalized CDCs (S_o/S_{orw} versus N_t) for both carbonate plugs and the Chatzis and Morrow [2] reference curve. In strongly water-wet media, residual oil is commonly trapped as discontinuous ganglia in larger pores through snap-off at pore constrictions [18,19], with mobilization over a relatively narrow threshold.

The sandstone reference in Fig. 3 uses values tabulated by Chatzis and Morrow [2] for 16 consolidated water-wet sandstones. To place their data on the same basis, their capillary number, $N_{c,2}$, was converted to the trapping-number definition used here. Chatzis and Morrow define $N_{c,2}$ using brine permeability (k_w) and the imposed pressure gradient: $N_{c,2} = k_w \Delta P/(L\sigma)$. Substituting Darcy's law for the aqueous

phase, u = krwkw/μ × ΔP/L, gives ΔP/L = uμ/(kwkrw) and therefore $N_{c,2}$ = uμ/(σkrw). The present trapping number uses the interstitial-velocity convention, N_t = uμ/(ϕσ) (Eq. (7)). Dividing N_t by $N_{c,2}$ gives $N_t = N_{c,2} \times (k_{rw}/\phi)$ (Eq. (8)). For Berea BL-2, which anchors the Chatzis dataset, k_{rw} at S_{orw} is 0.202 and ϕ is 0.225, giving a multiplier of ~0.9. This conversion is used only to place the onset comparison on a consistent basis; on an N_t axis spanning several orders of magnitude, log10(0.9) = −0.046 is visually negligible.

$$N_t = \frac{u\mu}{\phi\sigma} \tag{7}$$

$$N_t = N_{c,2} \times \left(\frac{k_{rw}}{\phi}\right) \tag{8}$$

The overlay shows that both tested carbonate systems require substantially higher mobilizing forces than the selected water-wet sandstone baseline. The 16 water-wet sandstones have a mean mobilization onset of $(1.9 \pm 0.6) \times 10^{-5}$. Core RC ($N_{t,crit} = 2.23 \times 10^{-3}$) is ~117× higher (2.07 log orders), and Core IL ($N_{t,crit} = 8.47 \times 10^{-4}$) is ~45× higher (1.65 log orders). Both thresholds exceed the +1 standard-deviation upper bound (2.5×10^{-5}). This comparison supports carbonate-specific CDC thresholds in screening calculations and cautions against direct transfer of water-wet sandstone criteria to aged or mixed-wet carbonates. Consistent with Humphry et al. [6], the magnitude of the shift is attributed primarily to wettability rather than sandstone–carbonate lithology contrast.

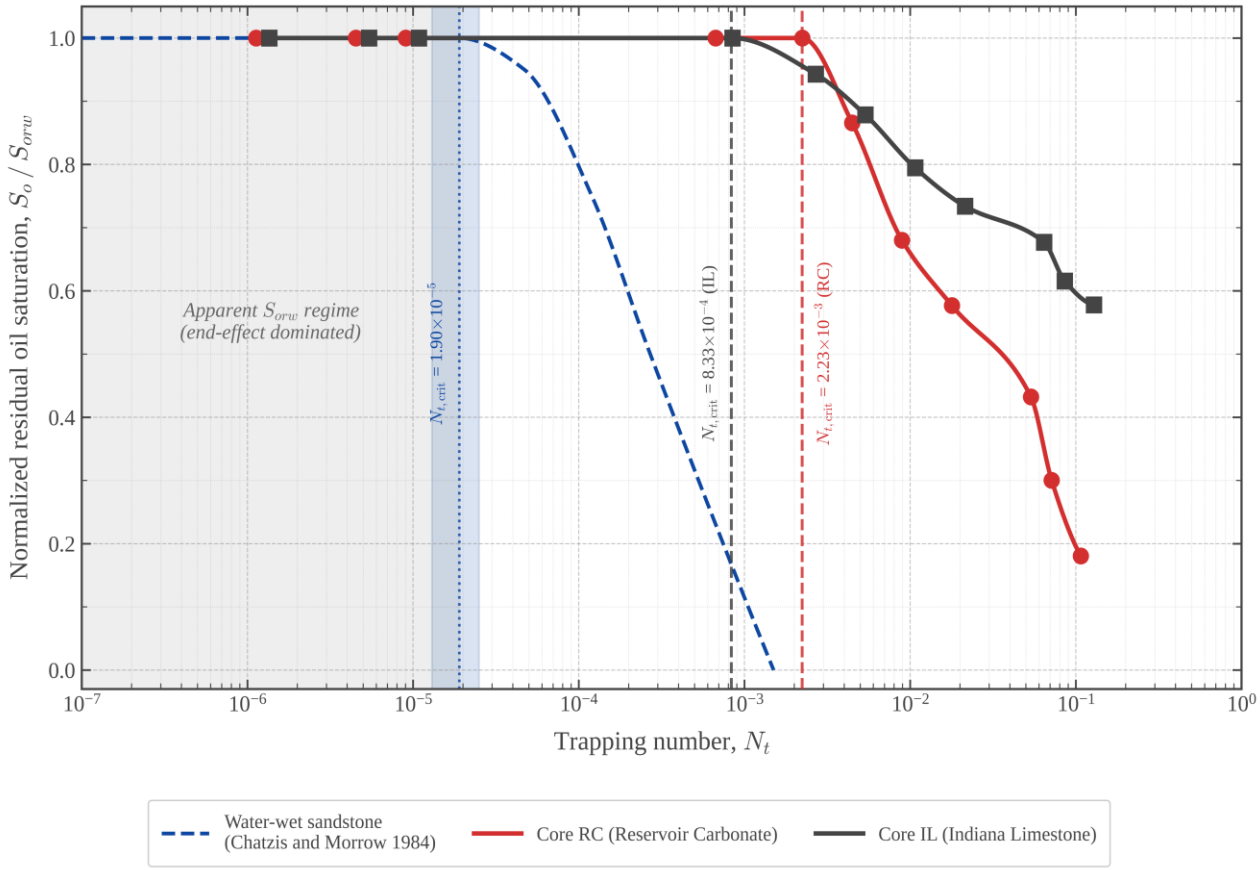

Fig. 3. Normalized CDCs for carbonate cores and the water-wet sandstone reference [2]. Curves are plotted as S_o/S_{orw} versus N_t under $\sigma_{os} = 3.07 \times 10^{-3}$ mN/m.

3.5. CDC Slope and Trapping Behavior. The rightward CDC shift is consistent with stronger capillary retention in the tested aged carbonate systems. In strongly water-wet sandstone systems, residual oil commonly occurs as disconnected ganglia in larger pores, and mobilization can occur over a relatively narrow interval once the critical threshold is exceeded [18,20].

In the tested aged carbonate plugs, delayed onset and more gradual desaturation are consistent with oil retained on rough carbonate surfaces, in microporosity, and in wetting films [5]. Because no pore-scale imaging was acquired, this interpretation is a mechanistic explanation consistent with the observed CDCs rather than direct evidence of pore-scale configuration.

The CDC slope provides qualitative diagnostic information about trapping behavior. Core RC shows a sharper transition immediately after $N_{t,crit}$, suggesting that a larger fraction of tertiary movable oil enters the mobilization window over a narrow N_t range. Core IL

shows a more gradual response over more than one order of magnitude in Nt, consistent with a broader distribution of accessible pore-scale trapping environments and macro-pore/micro-pore partitioning in complex carbonates [21]. Water-wet step-function CDC models can therefore overpredict the onset and efficiency of chemical mobilization when applied directly to the tested carbonate systems.

3.6. Salinity-Gradient Post-Flush Response. Fig. 4 summarizes normalized endpoint oil saturations (S_o/S_{orw}) across the primary experimental stages. After the maximum viscous pressure-gradient plateau (Q = 12 cm^3/min), a 50% diluted-salinity brine at Q = 0.25 cm^3/min reduced S_o in Core RC from 7.2% to 5.8%, whereas Core IL remained at 9.5%. This low-rate post-flush tested whether additional oil could be mobilized through salinity-driven phase behavior rather than increased mechanical forcing.

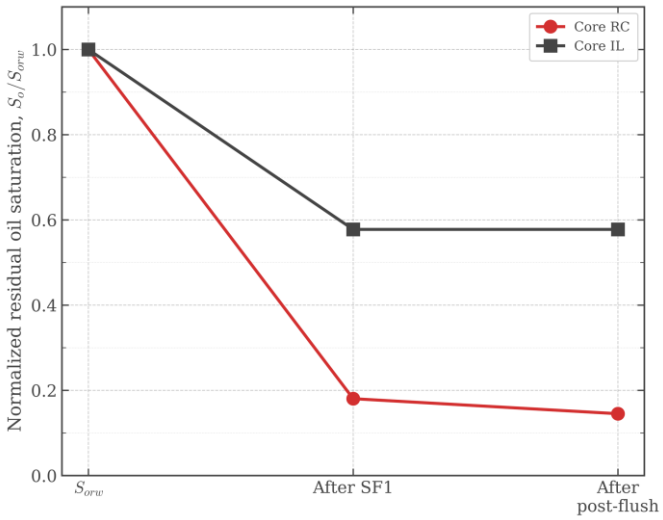

Fig. 4. Normalized endpoint oil saturations by experimental stage. Endpoints separate SF1 viscous desaturation from the low-rate salinity-gradient post-flush.

Because the late-stage mobilization in Core RC occurred at a low flow rate, the response is consistent with a phase-behavior contribution rather than increased viscous stress. Dilution can shift the local phase environment from optimum Winsor Type III toward an under-optimum water-soluble Winsor Type I state [13,14]. Similar engineered-brine/surfactant carbonate experiments show that brine composition, wettability alteration, Winsor III microemulsion behavior, and IFT reduction can act jointly during tertiary recovery [22].

This shift provides a plausible basis for resolubilization of trapped microemulsion or reduced interfacial-film stability, but the present data do not uniquely identify the mechanism. The absence of additional response in Core IL may reflect poorer access to remaining oil, different pore-scale trapping, or measurement-resolution limits.

Table 4 summarizes the measured petrophysical parameters, endpoint saturations, and microscopic displacement efficiencies for both corefloods.

Table 4. Summary of CDC Coreflooding Experiments

Parameter	Core RC (Reservoir)	Core IL (Outcrop)
Absolute permeability k_b	10.07 mD	97.58 mD
Effective permeability at S_{orw} ($k_{w,Sorw}$)	2.24 mD	74.93 mD
Porosity (ϕ)	0.22	0.18
Residual oil saturation after waterflood (S_{orw})	40%	16.5%
Critical trapping number ($N_{t,crit}$)	2.23×10^{-3}	8.47×10^{-4}
Final oil saturation after SF1 (S_{orc})	7.2%	9.5%
Final oil saturation after post-flush ($S_{o,post}$)	5.8%	9.5%
Microscopic displacement efficiency after SF1 (ED,SF1)	81.95%	42.22%
Microscopic displacement efficiency after post-flush ($E_{D,post}$)	85.48%	42.22%

3.7. Field-Rate Scaling and Viscosity Constraints. Translating the laboratory diagnostic limits into field-rate screening exposes the chemical-EOR challenge in the tested low-permeability carbonate. To evaluate feasibility, we assess the mobilizing force at a representative field Darcy velocity of u = 1 ft/day. Applying the aqueous viscosity (μ = 0.40 cP) and the extrapolated ultra-low IFT of

formulation SF1 (σ_{os}(100 °C) = 3.07 × 10^{-3} mN/m) for the reservoir rock (ϕ = 0.22) gives $N_t \approx 2.09 \times 10^{-3}$. This value is slightly below the measured Core RC onset ($N_{t,crit} = 2.23 \times 10^{-3}$), indicating that ultra-low IFT alone provides limited margin for initiating desaturation in the low-permeability reservoir plug under the adopted scaling. For Core IL, the measured threshold is lower ($N_{t,crit} = 8.47 \times 10^{-4}$), so the same field-rate scaling would exceed the IL onset threshold; however, IL is an outcrop analogue and should not be generalized as a reservoir prediction.

Fig. 5 translates the Core RC CDC into viscosity scaling at field Darcy velocities. Only a modest viscosity increase would be required to cross the Core RC onset threshold at u = 1 ft/day under the adopted calculation. Higher viscosities, on the order of ~2 cP and above, correspond to deeper desaturation targets near $N_t \approx 10^{-2}$ rather than onset alone. Under the HTHS conditions evaluated here (100 °C and 243,028 ppm TDS), polymer selection and propagation would require HTHS-stable chemistries, such as acrylamido tertiary butyl sulfonate (ATBS)-based synthetic polymers, rather than conventional hydrolyzed polyacrylamide (HPAM). Literature values indicate that achieving in situ viscosities of approximately 2 cP may require active polymer concentrations of 1,500–2,000 ppm, while reaching approximately 10 cP may require 3,500–4,000 ppm [23]. These values are used as viscosity screening targets; polymer rheology, retention, degradation, and propagation were not directly measured in this study.

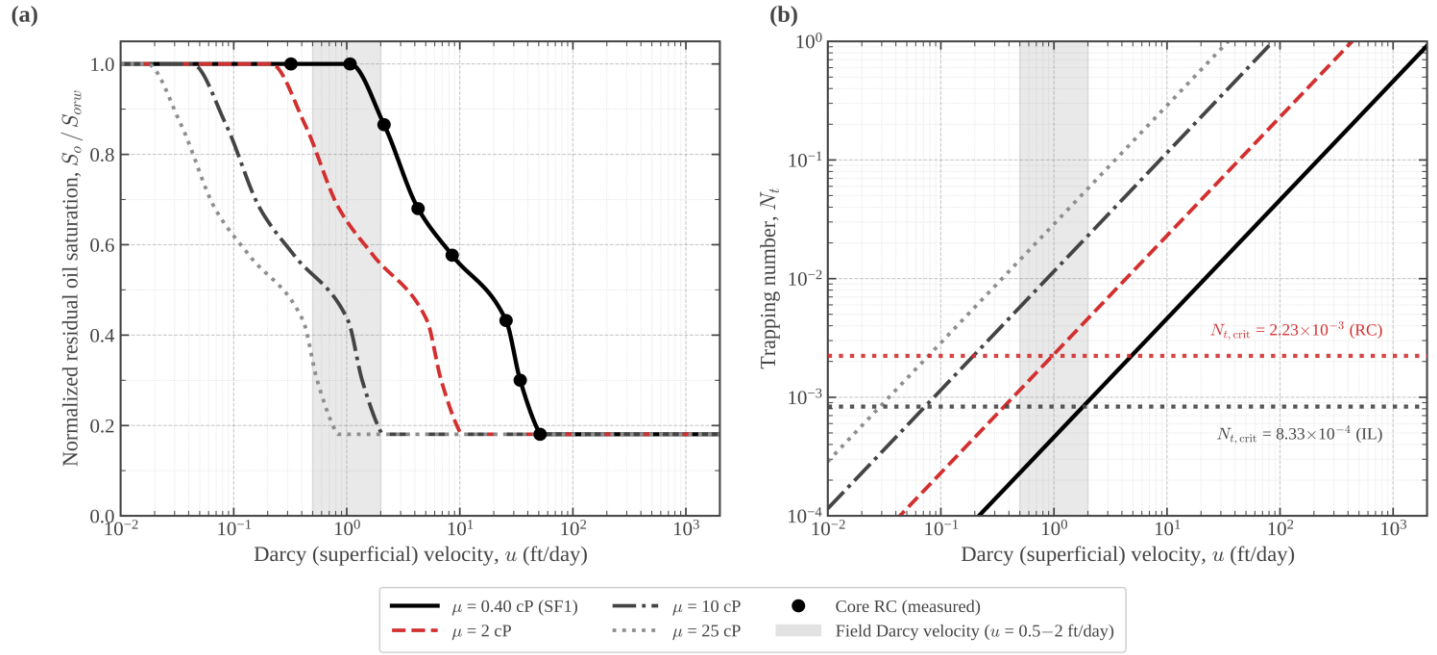

Fig. 5. Velocity–viscosity sensitivity for Core RC under ultra-low IFT. Panels show (a) S_o/S_{orw} and (b) N_t versus Darcy velocity; the shaded band indicates 0.5–2 ft/day.

Translating this viscosity requirement into field execution requires pressure-gradient and injectivity analysis. In low-permeability lithologies such as Core RC ($k_{w,Sorw} \approx 2.24$ mD), viscous polymer injection may be constrained by injectivity, mechanical degradation, filtration or face-plugging, and formation fracture-pressure limits. These constraints make the viscosity-injectivity trade-off a screening decision point for mature low-permeability carbonate fields, rather than a post hoc implementation detail. The present experiments do not directly measure these limits; therefore, the field implication is restricted to the identification of a likely implementation constraint.

In higher-permeability intervals—represented here only by the outcrop analogue (Core IL, $k_{w,Sorw} \approx 75$ mD)—viscosity enhancement would increase the calculated trapping number more readily at the same Darcy velocity. However, this does not establish that polymer solutions can be propagated without exceeding formation parting pressure or incurring unacceptable retention. The economic and technical viability of high-concentration polymer slugs depends on injectivity, polymer retention, shear stability, salinity tolerance, and adsorption on carbonate surfaces, all of which require separate evaluation before field design.

These field-rate implications should be read within the experimental limits of the study. The dataset comprises one reservoir plug (Core RC) and one outcrop analogue (Core IL), the wetting state is inferred rather than independently quantified as stated in Section 2.1, and the oil–surfactant IFT used in N_t calculations is extrapolated above 90 °C with uncertainty quantified in Section 2.3. In addition, $N_{t,crit}$ is an operational bracket defined by the highest tested trapping number before measurable desaturation and the next rate step that produced oil, rather than a continuously resolved onset.

4. Summary and Conclusions

Experimental characterization of capillary desaturation curves (CDCs) for a crude-oil-aged reservoir carbonate plug (Core RC) and an Indiana Limestone outcrop analogue (Core IL) at 100 °C under seawater injection (43,373 ppm TDS) supports the following conclusions:

- Residual-Oil Baseline Definition: Centrifuge conditioning established S_{orw} baselines of 40% for Core RC and 16.5% for Core IL; these reference values are protocol- and rock-dependent rather than universal residual saturations.
- Measured Carbonate Trapping Thresholds: The measured critical trapping numbers were $N_{t,crit} = 2.23 \times 10^{-3}$ for Core RC and 8.47×10^{-4} for Core IL; both exceed the selected water-wet sandstone reference, indicating larger mobilizing-force requirements in the tested aged carbonate plugs.
- Sandstone Benchmark and CDC Response: Core RC and Core IL showed 117× and 45× higher mobilization thresholds, respectively, than the selected sandstone onset; because only one reservoir plug and one outcrop analogue were tested, CDC slope differences remain sample-bounded.
- Field-Rate Scaling and Screening Implication: At u = 1 ft/day, the ultra-low-IFT formulation gives $N_t \approx 2.09 \times 10^{-3}$ for Core RC, slightly below onset; viscosity enhancement can provide additional margin toward deeper desaturation targets (e.g., $N_t \approx 10^{-2}$ at ~2 cP), but injectivity, polymer propagation, retention, salinity tolerance, and fracture-pressure constraints bound screening for mature HTHS carbonate reservoirs.

Nomenclature

Symbols

C	Huh constant, mN/m
E_D	Microscopic displacement efficiency, fraction
g	Gravitational acceleration, m/s²
k_b	Absolute (brine) permeability, mD
k_{rw}	Relative permeability to water, fraction
$k_{w,Sorw}$	Effective permeability to water at residual oil saturation, mD
L	Core plug length, cm
N_b	Bond number, dimensionless
N_c	Capillary number, dimensionless
$N_{c,2}$	Chatzis capillary number definition, dimensionless
N_t	Trapping number, dimensionless
$N_{t,crit}$	Critical trapping number, dimensionless
Q	Volumetric flow rate, cm³/min
R^*	Optimal solubilization ratio, cm³/cm³
S^*	Optimal salinity, ppm TDS
S_o	Oil saturation, fraction
S_{orc}	Residual oil saturation after chemical flood, fraction
S_{orw}	Residual oil saturation after waterflood, fraction
S_{wi}	Initial water saturation, fraction
u	Darcy (superficial) velocity, ft/day
v	Interstitial velocity, ft/day
v_{crit}	Critical interstitial velocity, ft/day

V_o Oil volume in middle phase, cm³

V_s Surfactant volume, cm³

V_w Water volume in middle phase, cm³

Greek letters

α Dip angle, degrees

$\Delta\rho$ Density difference between phases, kg/m³

ΔP Differential pressure, psi or Pa

ϕ Porosity, fraction

μ Aqueous displacing-phase viscosity, cP

σ_{Huh} IFT derived from Huh relation, mN/m

σ_{ow} Oil-water interfacial tension, mN/m

σ_{os} Oil-surfactant interfacial tension, mN/m

θ Contact angle, degrees

Abbreviations

ATBS Acrylamido tertiary butyl sulfonate

CDC Capillary Desaturation Curve

EOR Enhanced Oil Recovery

FW Formation Water

GAC Guerbet Alkoxy Carboxylate surfactant

HPAM Hydrolyzed polyacrylamide

HPHT High Pressure, High Temperature

HTHS High Temperature, High Salinity

IFT Interfacial Tension

IL Indiana Limestone outcrop core plug

IOS Internal Olefin Sulfonate surfactant

PV Pore Volume

RC Reservoir Carbonate core plug

SF1 Surfactant Formulation 1

SW Seawater

TDS Total Dissolved Solids

CRediT authorship contribution statement

Imad A. Adel: Conceptualization, Methodology, Data curation, Formal analysis, Investigation, Software, Visualization, Writing – original draft, Writing – review & editing. **Alvaro Hernandez Moralez:** Conceptualization, Investigation, Writing – review & editing. **Mohamed Efara:** Conceptualization, Investigation. **Emad W. Al-Shalabi:** Investigation, Project administration, Supervision, Writing – review & editing. **Ali AlSumaiti:** Conceptualization, Project administration, Supervision. **Shehadeh Masalmeh:** Conceptualization, Formal analysis, Investigation, Project administration, Supervision, Writing – review & editing.

Declaration of Competing Interest

The authors declare that they have no known competing financial interests or personal relationships that could have appeared to influence the work reported in this paper.

Data Availability Statement

Data supporting the findings of this study are available from the corresponding author upon reasonable request.

Acknowledgments

This research was funded by Khalifa University of Science and Technology through the ADNOC Grant Call under Project ID: KU-EXT-ADNOC-2022-8434000317. This research was supported by the Research and Innovation Center on CO_2 and Hydrogen, Khalifa University of Science and Technology (KU-RICH).

References

[1] A. Abrams, The influence of fluid viscosity, interfacial tension, and flow velocity on residual oil saturation left by waterflood, Soc. Pet. Eng. J. 15 (5) (1975) 437–447. https://doi.org/10.2118/5050-PA.

[2] I. Chatzis, N.R. Morrow, Correlation of capillary number relationships for sandstone, SPE J. 24 (5) (1984) 555–562. https://doi.org/10.2118/10114-PA.

[3] J.J. Sheng, Status of surfactant EOR technology, Petroleum 1 (2) (2015) 97–105. https://doi.org/10.1016/j.petlm.2015.07.003.

[4] P. Druetta, F. Picchioni, Surfactant flooding: The influence of the physical properties on the recovery efficiency, Petroleum 6 (2) (2020) 149–162. https://doi.org/10.1016/j.petlm.2019.07.001.

[5] S.K. Masalmeh, Determination of waterflooding residual oil saturation for mixed to oil-wet carbonate reservoir and its impact on EOR, in: SPE Reservoir Characterisation and Simulation Conference and Exhibition, Abu Dhabi, UAE, 16–18 September 2013, SPE-165981-MS. https://doi.org/10.2118/165981-MS.

[6] K.J. Humphry, B.M.J.M. Suijkerbuijk, H.A. van der Linde, S.G.J. Pieterse, S.K. Masalmeh, Impact of wettability on residual oil saturation and capillary desaturation curves, Petrophysics 55 (4) (2014) 313–318.

[7] S. Adkins, G.P.P. Arachchilage, S. Solairaj, J. Lu, U. Weerasooriya, G.A. Pope, Development of thermally and chemically stable large-hydrophobe alkoxy carboxylate surfactants, in: SPE Improved Oil Recovery Symposium, Tulsa, Oklahoma, USA, 14–18 April 2012, SPE-154256-MS. https://doi.org/10.2118/154256-MS.

[8] M.S. Kamal, I.A. Hussein, A.S. Sultan, Review on surfactant flooding: Phase behavior, retention, IFT, and field applications, Energy Fuels 31 (8) (2017) 7701–7720. https://doi.org/10.1021/acs.energyfuels.7b00353.

[9] D.J. O'Meara Jr., G.J. Hirasaki, J.A. Rohan, Centrifuge measurements of capillary pressure: Part 1—Outflow boundary condition, SPE Reserv. Eng. 7 (1) (1992) 133–142. https://doi.org/10.2118/18296-PA.

[10] D. Levitt, A.C. Jackson, C. Heinson, L.N. Britton, T. Malik, V. Dwarakanath, et al., Identification and evaluation of high-performance EOR surfactants, SPE Reserv. Eval. Eng. 12 (2) (2009) 243–253. https://doi.org/10.2118/100089-PA.

[11] V. Sahni, R.M. Dean, C. Britton, D.H. Kim, U. Weerasooriya, G.A. Pope, The role of co-solvents and co-surfactants in making chemical floods robust, in: SPE Improved Oil Recovery Symposium, Tulsa, Oklahoma, USA, 24–28 April 2010, SPE-130007-MS. https://doi.org/10.2118/130007-MS.

[12] G.A. Pope, W. Wu, G. Narayanaswamy, M. Delshad, M.M. Sharma, P. Wang, Modeling relative permeability effects in gas-condensate reservoirs with a new trapping model, SPE Reserv. Eval. Eng. 3 (2) (2000) 171–178. https://doi.org/10.2118/62497-PA.

[13] R.C. Nelson, G.A. Pope, Phase relationships in chemical flooding, SPE J. 18 (5) (1978) 325–338. https://doi.org/10.2118/6773-PA.

[14] G.J. Hirasaki, H.R. van Domselaar, R.C. Nelson, Evaluation of the salinity gradient concept in surfactant flooding, SPE J. 23 (3) (1983) 486–500. https://doi.org/10.2118/8825-PA.

[15] J. Lu, C. Britton, S. Solairaj, P.J. Liyanage, D.H. Kim, S. Adkins, et al., Novel large-hydrophobe alkoxy carboxylate surfactants for enhanced oil recovery, SPE J. 19 (6) (2014) 1024–1034. https://doi.org/10.2118/154261-PA.

[16] L.W. Lake, R. Johns, W.R. Rossen, G.A. Pope, Fundamentals of Enhanced Oil Recovery, Society of Petroleum Engineers, Richardson, Texas, 2014. https://doi.org/10.2118/9781613993286.

[17] C. Huh, Interfacial tensions and solubilizing ability of a microemulsion phase that coexists with oil and brine, J. Colloid Interface Sci. 71 (2) (1979) 408–426. https://doi.org/10.1016/0021-9797(79)90249-2.

[18] J.G. Roof, Snap-off of oil droplets in water-wet pores, SPE J. 10 (1) (1970) 85–90. https://doi.org/10.2118/2504-PA.

[19] N.R. Morrow, Interplay of capillary, viscous and buoyancy forces in the mobilization of residual oil, J. Can. Pet. Technol. 18 (3) (1979) 35–46. https://doi.org/10.2118/79-03-03.

[20] I. Chatzis, N.R. Morrow, H.T. Lim, Magnitude and detailed structure of residual oil saturation, SPE J. 23 (2) (1983) 311–326. https://doi.org/10.2118/10681-PA.

[21] E.A. Clerke, H.W. Mueller III, E.C. Phillips, R.Y. Eyvazzadeh, D.H. Jones, R. Ramamoorthy, et al., Application of Thomeer hyperbolas to decode the pore systems, facies and reservoir properties of the Upper Jurassic Arab D Limestone, Ghawar Field, Saudi Arabia: A Rosetta Stone approach, GeoArabia 13 (4) (2008) 113–160.

[22] A. Sekerbayeva, P. Pourafshary, M.R. Hashmet, Application of anionic surfactant/engineered water hybrid EOR in carbonate formations: An experimental analysis, Petroleum 8 (4) (2022) 466–475. https://doi.org/10.1016/j.petlm.2020.10.001.

[23] R.S. Seright, J.M. Seheult, T. Talashek, Injectivity characteristics of EOR polymers, SPE Reserv. Eval. Eng. 12 (5) (2009) 783–792. https://doi.org/10.2118/115142-PA.

[24] K. Al-Azani, S. Abu-Khamsin, M. Elsayed, S. Patil, S.M.S. Hussain, E. Al Shalabi, et al., Chemical enhanced oil recovery under harsh conditions: Investigation of rock permeability and insights from NMR measurements, Geoenergy Sci. Eng. 236 (2024) 212764. https://doi.org/10.1016/j.geoen.2024.212764.

[25] O. Massarweh, A.S. Abushaikha, Application of surfactants in enhancing oil recovery from tight carbonates: Physicochemical properties and core flooding experiments, Geoenergy Sci. Eng. 221 (2023) 211400. https://doi.org/10.1016/j.geoen.2022.211400.

[26] M. Souayeh, R.S. Al-Maamari, M. Karimi, M. Aoudia, Wettability alteration and oil recovery by surfactant assisted low salinity water in carbonate rock: The impact of nonionic/anionic surfactants, J. Pet. Sci. Eng. 197 (2021) 108108. https://doi.org/10.1016/j.petrol.2020.108108.